Chemical Science

Accepted Manuscript

This article can be cited before page numbers have been issued, to do this please use: W. Zhou, L. Wang, C. Liu, Q. Teng, Z. Wang and Z. Dai, *Chem. Sci.*, 2020, DOI: 10.1039/C9SC06408G.

ROYAL SOCIETY OF CHEMISTRY

rsc.li/chemical-science

View Article Online
DOI: 10.1039/C9SC06408G

ARTICLE

Quantification of Cyclic DNA Polymerization with Lanthanide Coordination Nanomaterials for Liquid Biopsy

Received 00th January 20xx,
Accepted 00th January 20xx

DOI: 10.1039/x0xx00000x

Wenting Zhou,[a] Lei Wang,[b] Can Liu,[a] Qiuyi Teng,[a] Zhaoyin Wang,*[a] and Zhihui Dai[ab]

Quantification of circulating tumor DNA (ctDNA) is of great importance in liquid biopsy but difficult for its low amount in bodily fluids. To meet this high demand, a novel method for ctDNA detection is established by quantifying cyclic DNA polymerization using lanthanide coordination polymers (Ln-CPs). Relying on the coordination between pyrophosphate ion (PPi) and trivalence cerium ion (Ce^{3+}), organic ligand-free PPi-Ce coordination polymer networks (PPi-Ce CPNs) with enhanced fluorescence are prepared for the first time. By surveying the optical properties of PPi-Ce CPNs, it is found that PPi regulates electric-dipole transition of Ce^{3+} to the lowest excited state, thus facilitating the emission of fluorescence. Therefore, fluorescence enhancement of PPi-Ce CPNs is originated from ligand field effect rather than normal antenna effect. Moreover, a new strategy to quantify DNA polymerization is developed based on PPi-Ce CPNs. By introducing multifold cyclic DNA polymerization, a small amount of ctDNA triggers the exponential generation of PPi to form plenty of PPi-Ce CPNs. Accordingly, a biosensor is constructed for sensitive ctDNA detection by measuring the intense fluorescence of PPi-Ce CPNs. The biosensor is capable of sensing ctDNA in sub-femtomolar, which is far better than analytical performances of commercial dyes. Besides, the analytical method is able to detect single nucleotide polymorphism and determine ctDNA in real samples. Considering DNA polymerization is widely used in bio-recognition, bio-assembly and biomineralization, the work provides a versatile quantitative strategy of making relevant processes precise and controllable.

Introduction

DNA polymerization is one of the most basic processes in living organisms.[1,2] In the past decades, various DNA polymerization-based approaches, including polymerase chain reaction (PCR) and nucleic acid isothermal amplification, have demonstrated their great value in molecular assembly,[3-5] target recognition,[6-8] and signal acquisition.[9,10] However, quantitative methods for DNA polymerization are still lacking in diversity. It is well known that the most remarkable outcome of DNA polymerization is generation of new DNA strands. Accordingly, current quantitative methods for DNA polymerization are mainly established by detecting the generated DNA strands (strand-based methods). In order to achieve quantification with these methods, generated DNA strands have to be stained with fluorescent probes in most cases.[10,11] Besides, fluorescent probes are normally toxic and thus unfriendly to experimental operations. Additionally, due to the insertion of fluorescent probes, the generated DNA strands are damaged and cannot be further used in subsequent applications. More importantly, fluorescent probes are sequence- or structure-dependent, and can only realize relative quantification. Therefore, strand-based methods are not able to compare and analyze polymerization of different DNA. Actually, besides DNA strands, pyrophosphate ion (PPi) is also produced as a by-product in the procedure of DNA polymerization.[12,13] Theoretically, the amount of produced PPi is much larger than that of generated DNA strands. If analytical methods are designed based on PPi, DNA polymerization is likely to be quantified more sensitively. Besides, PPi-based quantifications can be real-time, keeping the generated DNA strands undamaged. According to the basic principle of DNA polymerization, once DNA is polymerized, PPi will be produced. That is to say, PPi-based methods work in an absolute manner, which are tolerant of any sequence and structure.

Rare earth elements possess excellent luminescence properties owing to their special valence electron structures.[14,15] In particular, lanthanide (Ln) elements are capable of synthesizing luminescent materials with strong intensity, long lifetime and large Stokes shifts.[16-18] However, optical properties of pure Ln elements are greatly affected by solvents,[19,20] and even aqueous solution can quench Ln

[a] Jiangsu Collaborative Innovation Center of Biomedical Functional Materials and Jiangsu Key Laboratory of Biofunctional Materials, School of Chemistry and Materials Science, Nanjing Normal University, Nanjing, 210023, P. R. China. Tel./Fax: +86-25-85891051. E-mail: zywang@njnu.edu.cn.
[b] Nanjing Normal University Center for Analysis and Testing, Nanjing, 210023, P. R. China.

† Electronic Supplementary Information (ESI) available: Effect of PPi on the lifetime of Ce^{3+}, effect of ratio of PPi to Ce^{3+} and pH on fluorescence intensity of PPi-Ce CPNs, effect of ATP and dNTPs on fluorescence intensity of Ce^{3+}, optimization of detection conditions, fluorescence spectra obtained in different concentration of ctDNA, comparison of different methods for the determination of ctDNA and related references for supporting information. See DOI: 10.1039/x0xx00000x

DOI: 10.1039/C9SC06408G

elements due to the presence of OH groups.[21] Recently, lanthanide coordination polymers (Ln-CPs) have been developed to address the above issue.[22,23] In Ln-CPs, Ln elements are protected by coordination ligands against quench of solvents. Typically, organic ligands are employed to synthesize Ln-CPs and induce the enhancement of fluorescence by the so-called antenna effect.[24,25] For deficiencies in biocompatibility and biodegradability, these organic Ln-CPs are not suitable for bio-applications. To our knowledge, fluorescent Ln-CPs formed without organic ligands have not been reported to date.

In the process of tumor development, circulating tumor DNA (ctDNA) is released from cancer cells into the circulation system.[26] Since ctDNA contains the information of genome mutations, ctDNA has been considered as an ideal biomarker for liquid biopsy.[27] Notably, ctDNA comes from mutations of genome, which ensures the accuracy of ctDNA-based diagnosis.[28] Moreover, ctDNA can be directly obtained from bodily fluids, rendering detection of ctDNA simple and painless.[29] Although important, quantification of ctDNA in bodily fluids is difficult, mainly because the abundance of target ctDNA is low, while that of interferential DNA is high.[30] Currently, apart from digital PCR and targeted deep sequencing, some other methodologies including surface enhanced Raman scattering, electrochemistry, and localized surface plasmon resonance have been employed in detecting ctDNA.[31-35] However, the aforementioned methods still suffer from poor sensitivity. Therefore, more efforts should be devoted to propose new strategies of ctDNA detection.

Herein, organic ligand-free Ln-CPs with enhanced fluorescence were synthesized for the first time and employed in responses to ctDNA sensitively. By surveying the interactions between Ln elements and phosphate species, trivalence cerium ion (Ce^{3+}) and PPi were identified to prepare fluorescent PPi-Ce coordination polymer networks (PPi-Ce CPNs). Ligand field effect of PPi facilitated the energy transfer from the lowest excited state to the ground state of Ce^{3+}, resulting in the dramatic enhancement of fluorescence. During the procedure of DNA polymerization, PPi was accumulated to form PPi-Ce CPNs. Accordingly, quantification of DNA polymerization was achieved by measuring the fluorescence of formed PPi-Ce CPNs. The PPi-Ce CPNs-based quantitative strategy was further used to design a ctDNA biosensor. Benefitted from strong fluorescence of PPi-Ce CPNs and signal amplification of cyclic DNA polymerization, the biosensor was capable of detecting target ctDNA (KRAS G12DM, colon carcinoma-related ctDNA) in a wide linear range with a low detection limit. In addition, ctDNA in serum and wide DNA can also be determined accurately. Meanwhile, two commercial dyes were chosen to sense ctDNA as well. By comparing their analytical performances, it can be found that the detection limit of the proposed biosensor was at least eight orders of magnitude lower than that of commercial dyes.

Results and discussion

Principle of a fluorescent ctDNA biosensor based on cyclic DNA polymerization and PPi-Ce CPNs

Aiming to detect ctDNA at low concentration, a fluorescent biosensor was fabricated based on PPi-Ce CPNs and cyclic DNA polymerization. The biosensor consists of two DNA oligonucleotides, *i.e.*, primer DNA (P-DNA) and hairpin DNA (H-DNA), a polymerase (Klenow Fragment, KF) and a restriction endonuclease (Nt.BbvCI) (Fig. 1). H-DNA contains two domains: one is the complementary sequence of target ctDNA, while the other is the cut site of Nt.BbvCI. At the initial phase, H-DNA is self-hybridized. In this case, P-DNA cannot hybridize with H-DNA, thus impeding the initiation of DNA polymerization. However, ctDNA may induce the conformational change of H-DNA. Therefore, in the presence of ctDNA, P-DNA hybridizes with H-DNA and triggers the DNA polymerization under the participation of KF. As a result, P-DNA is lengthened, releasing ctDNA from H-DNA. At the same time, PPi, as the by-product of DNA polymerization, is accumulated (Part I). Released ctDNA can change the conformation of H-DNA once again, resulting in the cyclic DNA polymerization (Cycle I). Due to the elongation of P-DNA, the cleavage site in double-stranded H-DNA is recognized and cut by Nt.BbvCI, causing a nick in double-stranded H-DNA. In this case, P-DNA is further lengthened to achieve cyclic polymerization (Cycle II), releasing auxiliary DNA (A-DNA) and PPi (Part II). Released A-DNA works like ctDNA that can hybridize with H-DNA and initiate cyclic DNA polymerization (Cycle III and IV) with the aid of KF and Nt.BbvCI. During the Cycle III and IV, PPi is also produced (Part III and IV). Through the multifold cyclic DNA polymerization, lots of PPi from Part I, II, III and IV is accumulated, which is further employed to

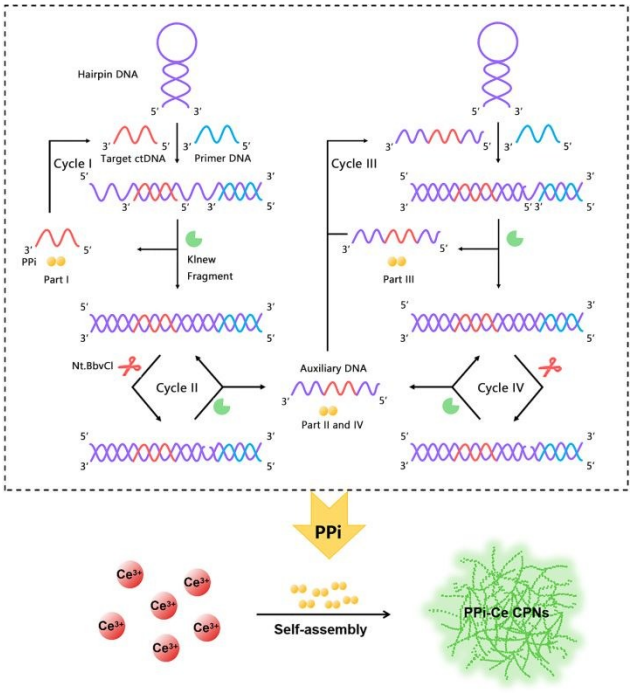

Fig. 1 Schematic illustration of ctDNA detection via quantification of cyclic DNA polymerization using PPi-Ce CPNs.

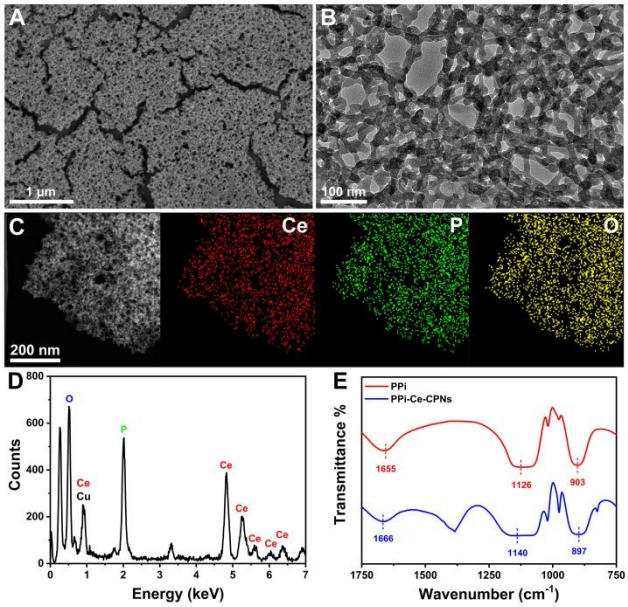

Fig. 2 (A) SEM and (B) TEM images of PPi-Ce CPNs. (C) STEM image of PPi-Ce CPNs and EDS mapping of Ce in red, P in green and O in yellow. (D) EDS spectrum of PPi-Ce CPNs. (E) FT-IR spectra of PPi and PPi-Ce CPNs.

prepare Ln CPs. Owing to coordination of PPi and Ce^{3+}, PPi-Ce CPNs are formed and emit strong fluorescence. Accordingly, by acquiring the signal from PPi-Ce CPNs, ctDNA is quantified sensitively.

Characterization of PPi-Ce CPNs

PPi-Ce CPNs were prepared by the self-assembly of PPi and Ce^{3+}, and morphology of the obtained PPi-Ce CPNs was firstly characterized with scanning electron microscopy (SEM) and transmission electron microscopy (TEM) images (Fig. 2A and B). PPi-Ce CPNs show a network structure, and abundant nodes with the diameter of about 15 nm can be found in the nanomaterials. In energy dispersive X-ray spectroscopy (EDS) spectrum, elementary peaks of Ce, P and O can be observed (Fig. 2D). Besides, scanning transmission electron microscope (STEM) image and EDS mapping indicate that Ce, P and O elements are uniformly distributed in PPi-Ce CPNs (Fig. 2C). In addition, Fourier transform infrared (FT-IR) spectra were recorded to investigate the formation of PPi-Ce CPNs (Fig. 2E). As reported in previous studies, the FT-IR peaks at 1655 cm^{-1}, 1126 cm^{-1} and 903 cm^{-1} represent P-OH stretching band (νP-OH), phosphate antisymmetric vibration bands ($\nu_{as}PO_3$), and phosphate symmetric vibration bands ($\nu_{s}PO_3$).[36,37] Relevant peaks in FT-IR spectrum of PPi-Ce CPNs emerge at 1666 cm^{-1}, 1140 cm^{-1} and 897 cm^{-1}, respectively. The shift of peak wavelength demonstrates that PPi interacts with Ce^{3+}, which provides the basis of the formation of PPi-Ce CPNs.

Optical properties of PPi-Ce CPNs

Optical properties of PPi-Ce CPNs were further studied with ultraviolet-visible (UV-vis) absorption and fluorescence spectrometry. Ce^{3+} reveals typical absorption peaks at 252 and 298 nm due to electric-dipole transitions of a ground state ($^2F_{5/2}$) to a doublet of excited states ($^2D_{5/2}$ and $^2D_{3/2}$) (Fig.

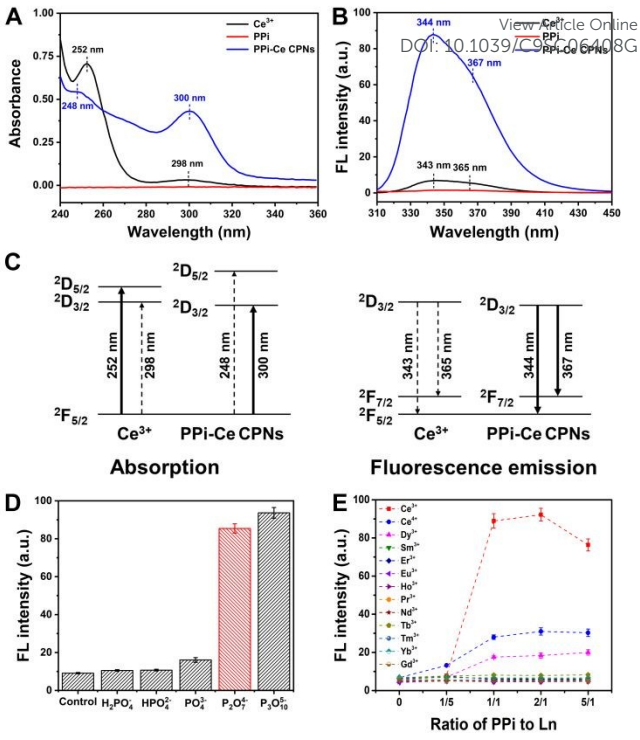

Fig. 3 (A) UV-vis absorption and (B) fluorescence spectra of Ce^{3+}, PPi and PPi-Ce CPNs. (C) Schematic energy level diagram and energy transfer process in absorption and fluorescence emission of Ce^{3+} and PPi-Ce CPNs. (D) Fluorescence intensity of Ce^{3+} mixed with different phosphate species. (E) Fluorescence intensity of PPi mixed with different Ln elements.

3A).[38] Contrary to Ce^{3+}, there is no peak in the absorption spectrum of PPi. However, by mixing Ce^{3+} with PPi, the absorption at 298 nm is dramatically increased in accompany with a slight red-shift, while the peak at 252 nm is depressed with a blue-shift. The results indicate that ligand field effect of PPi generates a larger energy difference of $^2D_{5/2}$ and $^2D_{3/2}$ excited states of Ce^{3+}. Therefore, energy difference between $^2F_{5/2}$ and $^2D_{3/2}$ is decreased, resulting in the red-shift of the peak at 298 nm, while energy difference between $^2F_{5/2}$ and $^2D_{5/2}$ is increased, leading to blue-shift of the peak at 252 nm. Meanwhile, the electric-dipole transition to a low excited state ($^2D_{3/2}$) is greatly promoted, and the transition to a high excited state ($^2D_{5/2}$) is impeded. Furthermore, it is found that the fluorescence of Ce^{3+} is evidently enhanced (about 10 times) by the formation of PPi-Ce CPNs in accompany with the reduction of average lifetime. (Fig. 3B and S1 †). As demonstrated above, ligand field effect of PPi promotes the transition from $^2F_{5/2}$ to $^2D_{3/2}$. Accordingly, more Ce^{3+} reaches to the lowest excited state ($^2D_{3/2}$). Therefore, energy loss of nonradiative transition from $^2D_{5/2}$ to $^2D_{3/2}$ is reduced. Spontaneously, radiative transition from $^2D_{3/2}$ to ground states ($^2F_{7/2}$ and $^2F_{5/2}$) is facilitated, rendering the fluorescence enhancement of Ce^{3+}. The relevant energy level diagram and energy transfer process in absorption and fluorescence emission of Ce^{3+} and PPi-Ce CPNs are illustrated in Fig. 3C. Fig. S2 † depicts the correlation between fluorescence intensity of PPi-Ce CPNs and ratio of PPi to Ce^{3+}. With the increase of PPi, more PPi-Ce CPNs are assembled,

View Article Online DOI: 10.1039/C9SC06198G

leading to the enhancement of fluorescence. However, if excessive PPi is employed, PPi-Ce CPNs may be destructed, causing the decrease of fluorescence. On a basis of our data, equimolar PPi and Ce^{3+} is the optimal ratio to obtain intense fluorescence emission. Under the similar condition, effects of phosphate species on fluorescence of Ce^{3+} were studied. As shown in Fig. 3D, PPi and $P_3O_{10}^{5-}$ can enhance fluorescence of Ce^{3+}, while effects of $H_2PO_4^-$, HPO_4^{2-} and PO_4^{3-} are negligible. In comparison with monophosphates, polyphosphates possess more terminal phosphates and negative charges, thus enhancing binding affinity and electrostatic field intensity of ligands.[39] Considering that ligand field effect is highly relevant to binding affinity and electrostatic field intensity of ligand, enhancement of fluorescence has a positive correlation with the number of phosphate group in phosphate species, and polyphosphates are essential to form Ce-based coordination polymers with strong fluorescence. To investigate the effect of pH on the fluorescence of Ce^{3+}, PPi-Ce CPNs are prepared under different pH values (from 5 to 10). In these cases, fluorescence of formed PPi-Ce CPNs is steady (Fig. S3), indicating that fluorescence enhancement of Ce^{3+} caused by PPi is independent on the pH of the solution. It is reported that ATP can also be used to form polymers with Ce^{3+}.[22,40,41] Actually, in these studies, polymers are prepared in the presence of ATP as well as tris(hydroxymethyl)aminomethane (Tris), and Tris plays a key role in regulating the fluorescence of Ce^{3+} depending on antenna effect. If Tris is absent, ATP can only induce a slight fluorescence enhancement (Fig. S4). In contrast, by replacing ATP with PPi, fluorescence of Ce^{3+} can be significantly increased due to ligand field effect. In addition to Ce^{3+}, other Ln elements (except for non-fluorescent La^{3+} and Lu^{3+}, and radioactive Pm^{3+}) are employed to assemble coordination polymers with PPi. According to the fluorescence of different PPi-Ln mixtures (Fig. 3E), only Ce^{3+} can be coupled with PPi to form fluorescent Ln-CPs, which should be attributed to the special electron structure of Ce^{3+} and ligand field effect of PPi.

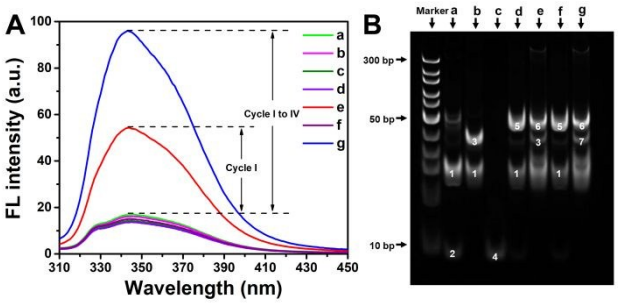

Fig. 4 (A) Fluorescence spectra and (B) PAGE image obtained under different conditions: (a) H-DNA, P-DNA, KF and Nt.BbvCI, (b) H-DNA, ctDNA, KF and Nt.BbvCI, (c) P-DNA, ctDNA, KF and Nt.BbvCI, (d) H-DNA, P-DNA and ctDNA, (e) H-DNA, P-DNA, ctDNA, and KF, (f) H-DNA, P-DNA, ctDNA, and Nt.BbvCI, and (g) H-DNA, P-DNA, ctDNA, KF and Nt.BbvCI.

Feasibility of the bioanalytical method

In order to testify the feasibility of the designed method, fluorescence spectra under different conditions were recorded (Fig. 4A). As expected, in the absence of ctDNA, P-DNA, H-DNA or KF, DNA amplification is impeded. In these cases, PPi is not produced, and thus PPi-Ce CPNs are not formed. Therefore, only weak background fluorescence of Ce3+ can be detected (curves a, b, c, d and f in Fig. 4A). In the presence of all reactants but Nt.BbvCI, one of multifold cyclic DNA polymerization (Cycle I) is triggered, while Cycle II, III and IV are still blocked. As a result, part of PPi (Part I) is accumulated to form PPi-Ce CPNs that emit enhanced fluorescence (curve e in Fig. 4A). However, if all reactants are present, ctDNA initiates multifold cyclic DNA polymerization that produces a large amount of PPi from Part I, II, III and IV. Theoretically, approximate ratio of PPi/DNA strand is 28, since lengths of H-DNA and P-DNA are 43 and 15 nt, respectively. Accordingly, plenty of PPi-Ce CPNs are prepared and intense fluorescence is obtained (curve g in Fig. 4A). As shown in Fig. S5, effect of dNTPs on fluorescence of Ce^{3+} is slight. Accordingly, ctDNA can be accurately determined without purification to remove excess dNTPs. Electrophoresis was further carried out to study the detection process in the view of DNA operation (Fig. 4B). In polyacrylamide gel electrophoresis (PAGE) image, band 1 and 2 in lane a represent H-DNA and P-DNA respectively. In the presence of ctDNA, band 3 appears in lane b, manifesting the hybridization of ctDNA and H-DNA. The mixture of P-DNA and ctDNA results in band 4 in lane c. In lane d, conformation of

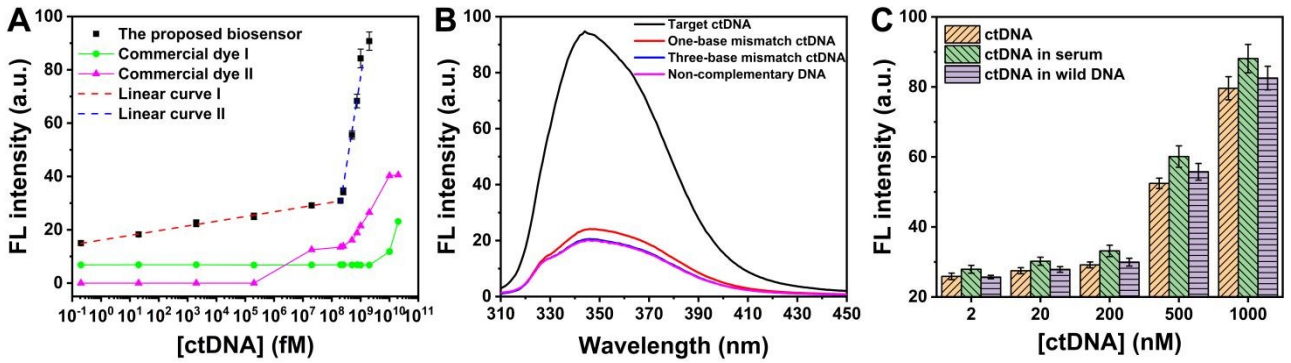

Fig. 5 (A) Fluorescence responses of the proposed biosensor, commercial dye I (4S Red Plus Nucleic Acid Stain) and commercial dye II (ssDNA Dye) to various concentrations of ctDNA. (B) Fluorescence intensity of the biosensor in response to ctDNA, one-base mismatch ctDNA, three-base mismatch ctDNA and non-complementary DNA. The concentration of different DNA is 2 μM. (C) Detection of pure ctDNA, ctDNA in 1% serum and ctDNA in 2 μM wild DNA with the proposed biosensor.

View Article Online
DOI: 10.1039/C9SC06408C

H-DNA is changed by ctDNA. Accordingly, ctDNA and P-DNA can co-hybridize with H-DNA, leading to the appearance of band 5. In lane e, KF causes the elongation of P-DNA, forming the double-stranded H-DNA. Consequently, a new band (band 6) emerges in lane e. In the presence of Nt.BbvCI, A-DNA is obtained by cutting in the cleavage site of double-stranded H-DNA. The band 7 in lane g should be attributed to the hybridization of A-DNA and H-DNA. The above results demonstrate that ctDNA can trigger cyclic DNA polymerization, leading to the generation of PPi-Ce CPNs. Therefore, ctDNA can be sensitively quantified by the fluorescence of PPi-Ce CPNs.

Analytical performances of the proposed biosensor

To pursue better analytical performances, dNTPs, KF and Nt.BbvCI used in the biosensor were optimized (Fig. S6A-C†). Meanwhile, 120 min was chosen as the best incubation time to detect ctDNA (Fig. S6D†). Under the optimal conditions, with the increase of ctDNA, more PPi is produced to form PPi-Ce CPNs, leading to the increase of fluorescence (Fig. S7†). As shown in Fig. 5A, fluorescence intensity of PPi-Ce CPNs at 344 nm ($F_{344\ nm}$) is proportional to the concentration of ctDNA ([ctDNA]) in a wide range. In the range from 0.2 fM to 200 nM, the linear regression equation is $F_{344\ nm} = 1.67\ lg^{[ctDNA]\ (fM)} + 15.2$ with a correlation coefficient (R) of 0.998. In the range from 200 nM to 1 μM, the linear regression equation is $F_{344\ nm} = 64.2\ lg^{[ctDNA]\ (fM)} - 505$ (R = 0.992). According to the parameters in the low concentration region (<200 nM), detection limit of this biosensor is calculated to be 0.16 fM (S/N = 3). As aforementioned, quantification of DNA polymerization is normally achieved based on the detection of generated DNA strands using commercial dyes. In this work, two kinds of commercial dyes (4S Red Plus Nucleic Acid Stain and ssDNADye) were employed to detect the same ctDNA. Although commercial dyes can also respond to ctDNA, fluorescence enhancement is observed only at high concentration. Detection limit of the biosensor is eight orders of magnitude lower than that of commercial dyes. To be noted, besides commercial dyes, detection limit and linear range of this biosensor is better than or at least comparable to those of different ctDNA biosensors (Table S1).

Besides ctDNA, three other DNA sequences including one-base mismatch ctDNA, three-base mismatch ctDNA and non-complementary DNA were chosen to challenge the proposed biosensor. According to the data shown in Fig. 5B, even one base mutation in ctDNA cannot induce significant fluorescence enhancement, demonstrating that the biosensor is capable of single nucleotide polymorphism detection. In combination with the data in Fig. 5A, it can be concluded that to obtain equal intensity, the concentration of mismatch DNA is 1 million times higher than that of ctDNA. The excellent selectivity should be ascribed to the strict Watson-Crick complementary matching principle and super-specific recognition function of restriction endonuclease. In practical applications, detection of ctDNA is often confronted with serious interferential components such as proteins and oligonucleotides. Accordingly, performances of determining ctDNA in human serum and wild DNA were studied (Fig. 5C). Although components of serum are complex, ctDNA in serum can still be detected accurately using our methods. Similar results are obtained in the case that concentration of interferential DNA is 100 times higher than that of ctDNA. Apart from low detection limit, wide linear range and satisfactory selectivity, the fluorescent biosensor possesses other strengths, such as simple operation, low cost and free of modification, suggesting great potential of this bioanalytical platform in liquid biopsy.

Conclusions

In summary, a new type of Ln-CPs is prepared according to the self-assembly of PPi and Ce^{3+}. Besides novel morphology, the PPi-Ce CPNs are able to emit strong fluorescence. Different from former Ln-CPs, optical properties of PPi-Ce CPNs are promoted without the participation of organic ligands, and the fluorescence enhancement is the result of ligand field effect rather than antenna effect. Based on these findings, a PPi-Ce CPNs-based method is established to quantify DNA polymerization. Since the amount of produced PPi is much larger than that of generated strands in the procedure of DNA polymerization, the PPi-Ce CPNs-based approach reveals overwhelming superiority over strand-based methods in sensitivity and versatility. To make full use of the excellent properties of PPi-Ce CPNs, a biosensor is further fabricated in a combination of multifold cyclic DNA polymerization. Benefitted from intense fluorescence of PPi-Ce CPNs and signal amplification of cyclic DNA polymerization, ctDNA in the range from 0.2 fM to 1 μM can be detected, which is valuable in ctDNA-based clinical diagnosis. Meanwhile, single nucleotide polymorphism of ctDNA and ctDNA in real samples can be accurately determined with the designed biosensor. Relying on the quantitative strategy proposed in this work, various PPi-related processes can be controlled and utilized precisely, which is of great significance in biomedicine and biotechnology.

Experimental

Chemicals and materials

Cerium nitrate hexahydrate ($Ce(NO_3)_3{\cdot}6H_2O$), holmium nitrate pentahydrate ($Ho(NO_3)_3{\cdot}5H_2O$), samarium nitrate hexahydrate ($Sm(NO_3)_3{\cdot}6H_2O$), erbium nitrate hexahydrate ($Er(NO_3)_3{\cdot}6H_2O$), dysprosium nitrate hexahydrate ($Dy(NO_3)_3{\cdot}6H_2O$), europium nitrate hexahydrate ($Eu(NO_3)_3{\cdot}6H_2O$), cerous sulphate ($Ce(SO_4)_2$), terbium nitrate hexahydrate ($Tb(NO_3)_3{\cdot}6H_2O$), Thulium nitrate pentahydrate ($Tm(NO_3)_3{\cdot}5H_2O$), Ytterbium nitrate pentahydrate, ($Yb(NO_3)_3{\cdot}5H_2O$), potassium pyrophosphate ($K_4P_2O_7$), mono-potassium phosphate (KH_2PO_4), di-potassium phosphate (K_2HPO_4), potassium phosphate (K_3PO_4), sodium tripolyphosphate ($Na_5P_3O_{10}$), and deoxy-ribonucleoside triphosphates (dNTPs) were obtained from Sigma-Aldrich Co., Ltd. (China). Praseodymium nitrate hexahydrate ($Pr(NO_3)_3{\cdot}6H_2O$), Neodymium nitrate hexahydrate

$(Nd(NO_3)_3{\cdot}6H_2O)$, Gadolinium nitrate hexahydrate $(Gd(NO_3)_3{\cdot}6H_2O)$, were obtained from Aladdin Bio-Chem Technology Co., Ltd. (Shanghai , China). Klenow Fragment (KF) and Nt.BbvCI were provided by New England Biolabs (NEB) Ltd. (Beijing, China). 4S Red Plus Nucleic Acid Stain (1000×) was obtained from Shanghai Sangon Biological Engineering Technology and Services Co., Ltd. (China). Single-stranded DNA (ssDNA) Dye was obtained from Promega Biotech Co., Ltd. (Beijing, China). All other reagents in this experiment were of analytical grade, and used directly without extra purification.

Oligonucleotides used in this work were synthesized and purified with HPLC by Shanghai Sangon Biological Engineering Technology and Services Co., Ltd. (China). Detail sequences of these oligonucleotides are shown in Table 1.

Apparatus

The fluorescence spectra were recorded by a Fluoromax-4 spectrometer (Horiba, France). The fluorescence emission spectra of trivalence cerium ion (Ce^{3+}) and PPi-Ce CPNs were measured from 310 to 450 nm with an excitation wavelength of 295 nm. The scanning electron microscopy (SEM) image was obtained on a JEOL JSM-7600F instrument (Japan). The transmission electron microscopy (TEM) image, scanning transmission electron microscope (STEM) image and energy dispersive X-ray spectroscopy (EDS) mapping were obtained on a JEM-200CX (200 kV) instrument (Japan). Polyacrylamide gel electrophoresis (PAGE) was obtained by a Model DYY-8C electrophoretic device. Fourier transform infrared (FT-IR) spectra were obtained by a gas chromatography Fourier transform infrared spectrometer (NEXUS670). Ultraviolet-visible (UV-vis) absorption spectra were measured with a Cary 60 spectrophotometer (Agilent, USA).

Interactions between Ln elements and phosphate species

On one hand, the interactions between Ce^{3+} and phosphate species were studied by mixing 20 μL of 0.5 mM $Ce(NO_3)_3{\cdot}6H_2O$ with 10 μL of 1 mM KH_2PO_4 (pH 5.68), K_2HPO_4 (pH 8.37), K_3PO_4 (pH 10.94), $K_4P_2O_7$ (pH 9.74) and $Na_5P_3O_{10}$ (pH 9.81), respectively. On the other hand, to investigate the interactions between pyrophosphate ion and Ln elements, 10 μL of 1 mM $K_4P_2O_7$ was mixed with 20 μL of 0.5 mM $Dy(NO_3)_3{\cdot}6H_2O$, $Sm(NO_3)_3{\cdot}6H_2O$, $Er(NO_3)_3{\cdot}6H_2O$, $Eu(NO_3)_3{\cdot}6H_2O$, $Ho(NO_3)_3{\cdot}5H_2O$, $Ce(SO_4)_2$, $Pr(NO_3)_3{\cdot}6H_2O$, $Nd(NO_3)_3{\cdot}6H_2O$, $Tb(NO_3)_3{\cdot}6H_2O$, $Tm(NO_3)_3{\cdot}5H_2O$, $Yb(NO_3)_3{\cdot}5H_2O$ and $Gd(NO_3)_3{\cdot}6H_2O$, respectively. After filled up to 300 μL with ultrapure water, these compounds were kept at room temperature for 15 minutes. Finally, fluorescence spectra of above samples were recorded.

Table 1. DNA sequences used in this work.

Name	Sequence from 5' to 3'
Hairpin DNA (H-DNA)	TCAGAC**GGAGCTGAT**GGCGTAGCTGAGG*ATC AGCTCCGTCTGA*
Primer DNA (P-DNA)	TCAGACGGAGCTGAT
Target ctDNA	TACGCCATCAGCTCC
One-base mismatch ctDNA	TACGCCAACAGCTCC
Three-base mismatch ctDNA	TACACCAACAGATCC
Non-complementary DNA	TACGACTCACTATAG

The sequence used to form hairpin structure was underlined. The italic and bold sequences were used to hybridize with P-DNA and ctDNA, respectively. The mismatch bases were marked with wavy line.

Construction of a fluorescent ctDNA biosensor

The biosensor was constructed based on cyclic DNA polymerization and PPi-Ce CPNs. First, the H-DNA was dissolved in 10 mM Tris-HCl (pH 7.6, 500 mM NaCl, 100 mM $MgCl_2$). Then the H-DNA solution was heated at 95 °C for 3 min, and cooled down gently to roomtemperature to form a hairpin structure. After that, DNA cyclic polymerization was carried out in a series of 100 μL solutions containing 3 μM H-DNA, 2 μM P-DNA, 50 μM dNTPs, 2 U KF, 1.5 U Nt.BbvCI, and different concentrations of ctDNA. After incubated at 37 °C for 2 hours, each of these solutions was mixed with 180 μL of 25 μM $Ce(NO_3)_3{\cdot}6H_2O$. After that, PPi-Ce CPNs were prepared by keeping these solutions at room temperature for 15 min. Finally, to achieve quantification of ctDNA, fluorescence spectrum of each sample was obtained under the excitation light of 295 nm.

To verify the selectivity of the biosensor, three other DNA (one-base mismatch ctDNA, three-base mismatch ctDNA and non-complementary DNA) were employed to replace ctDNA, and detected with the PPi-Ce CPNs-based quantitative method. To verify the analytical performances of the biosensor, two commercial dyes, *i.e.*, 4S Red Plus Nucleic Acid Stain and ssDNA Dye, were chosen to detect the same ctDNA. Various concentrations of ctDNA were mixed with 100× 4S Red Plus Nucleic Acid Stain and 1% ssDNA Dye, respectively. These solutions were incubated at room temperature for 15 min, and then fluorescence spectra of samples were recorded with an excitation wavelength of 300 or 492 nm. Applicability of the analytical method was clarified by detecting ctDNA in real samples. To be specific, different concentrations of ctDNA were diluted with 1% human serum and 2 μM wild DNA, respectively. Subsequently, ctDNA in real samples was quantified by the proposed biosensor.

Conflicts of interest

There are no conflicts of interest to declare.

Acknowledgements

This work was supported by the National Natural Science Foundation of China for the projects (Nos. 21625502 and 21974070) and Natural Science Foundation of Jiangsu Province of China (Nos. BK20192008 and BK20191367). All experiments involving human serum were performed in accordance with the guidelines of Safety and Welfare of Human Research of Nanjing Normal University and approved by the Ethics Committee of Nanjing Normal University. Informed consent was obtained from human participants of this study.

Notes and references

1 C. Marchal, J. Sima and D. M. Gilbert, *Nat. Rev. Mol. Cell Biol.*, 2019, DOI: 10.1038/s41580-019-0162-y.

2 J. Kottur and D. T. Nair, *Nucleic Acids Res.*, 2018, **46**, 5875-5885.
3 S. Li, L. Xu, W. Ma, X. Wu, M. Sun, H. Kuang, L. Wang, N. A. Kotov and C. Xu, *J. Am. Chem. Soc.*, 2016, **138**, 306-312.
4 S. Tanwar, K. K. Haldar and T. Sen, *J. Am. Chem. Soc.*, 2017, **139**, 17639-17648.
5 Y. Liu, X. Hu, T. Fu, R. Wang and W. Tan, *Sci. China: Chem.*, 2019, **62**, 407-408.
6 R. Yamashige, M. Kimoto, R. Okumura and I. Hirao, *J. Am. Chem. Soc.*, 2018, **140**, 14038-14041.
7 N. Melnychuk and A. S. Klymchenko, *J. Am. Chem. Soc.*, 2018, **140**, 10856-10865.
8 X. Wang, F. Chen, D. Zhang, Y. Zhao, J. Wei, L. Wang, S. Song, C. Fan and Y. Zhao, *Chem. Sci.*, 2017, **8**, 4764-4770.
9 M. G. Mohsen, D. Ji and E. T. Kool, *Chem. Sci.*, 2019, **10**, 3264-3270.
10 L. J. Wang, X. Han, C. C. Li and C. Y. Zhang, *Chem. Sci.*, 2018, **9**, 6053-6061.
11 C. C. Li, W. X. Liu, J. Hu and C. Y. Zhang, *Chem. Sci.*, 2019, **10**, 8675-8684.
12 T. Nakamura, Y. Zhao, Y. Yamagata, Y. J. Hua and W. Yang, *Nature*, 2012, **487**, 196-201.
13 L. T. Da, D. Wang and X. Huang, *J. Am. Chem. Soc.*, 2012, **134**, 2399-2406.
14 L. Dai, W. S. Lo, Y. Gu, Q. Xiong, K. L. Wong, W. M. Kwok, W. T. Wong and G. L. Law, *Chem. Sci.*, 2019, **10,** 4550-4559.
15 M. Hatanaka, Y. Hirai, Y. Kitagawa, T. Nakanishi, Y. Hasegawa and K. Morokuma, *Chem. Sci.*, 2017, **8**, 423-429.
16 F. Chen, Y. M. Wang, W. Guo and X. B. Yin, *Chem. Sci.*, 2019, **10**, 1644-1650.
17 J. Y. Hu, Y. Ning, Y. S. Meng, J. Zhang, Z. Y. Wu, S. Gao and J. L. Zhang, *Chem. Sci.*, 2017, **8**, 2702-2709.
18 W. Zhou, Y. Chen, Q. Yu, P. Li, X. Chen and Y. Liu, *Chem. Sci.*, 2019, **10**, 3346-3352.
19 X. L. Zheng, Y. Liu, M. Pan, X. Q. Lu, J. Y. Zhang, C. Y. Zhao, Y. X. Tong and C. Y. Su, *Angew. Chem. Int. Ed.*, 2007, **46**, 7399-7403.
20 C. L. Liu, R. L. Zhang, C. S. Lin, L. P. Zhou, L. X. Cai, J. T. Kong, S. Q. Yang, K. L. Han and Q. F. Sun, *J. Am. Chem. Soc.*, 2017, **139**, 12474-12479.
21 O. Guzman-Mendez, F. Gonzalez, S. Bernes, M. Flores-Alamo, J. Ordonez-Hernandez, H. Garcia-Ortega, J. Guerrero, W. Qian, N. Aliaga-Alcalde and L. Gasque, *Inorg. Chem.*, 2018, **57**, 908-911.
22 H. H. Zeng, W. B. Qiu, L. Zhang, R. P. Liang and J. D. Qiu, *Anal. Chem.*, 2016, **88**, 6342-6348;
23 X. Wu, Q. DeGottardi, I. C. Wu, J. Yu, L. Wu, F. Ye, C. T. Kuo, W. W. Kwok and D. T. Chiu, *Angew. Chem. Int. Ed.*, 2017, **56**, 14908-14912.
24 Y. Hirai, T. Nakanishi, Y. Kitagawa, K. Fushimi, T. Seki, H. Ito and Y. Hasegawa, *Angew. Chem. Int. Ed.*, 2017, **56**, 7171-7175.
25 Y. Hirai, T. Nakanishi, Y. Kitagawa, K. Fushimi, T. Seki, H. Ito and Y. Hasegawa, *Angew. Chem. Int. Ed.*, 2016, **55**, 12059-12062.
26 C. Abbosh, N. J. Birkbak and C. Swanton, *Nat. Rev. Clin. Oncol.*, 2018, **15**, 577-586.
27 J. Wang, K. M. Koo, Y. Wang and M. Trau, *Adv. Sci.*, 2019, DOI: 10.1002/advs.201900730, 1900730.
28 L. A. Diaz, Jr. and A. Bardelli, *J. Clin. Oncol.*, 2014, **32**, 579-586.
29 E. Heitzer, I. S. Haque, C. E. S. Roberts and M. R. Speicher, *Nat. Rev. Genet.*, 2019, **20**, 71-88.
30 J. Das, I. Ivanov, T. S. Safaei, E. H. Sargent and S. O. Kelley, *Angew. Chem. Int. Ed.*, 2018, **57**, 3711-3716.
31 A. M. Newman, S. V. Bratman, J. To, J. F. Wynne, N. C. Eclov, L. A. Modlin, C. L. Liu, J. W. Neal, H. A. Wakelee, R. E. Merritt, J. B. Shrager, B. W. Loo, Jr., A. A. Alizadeh and M. Diehn, *Nat. Med.*, 2014, **20**, 548-554.
32 M. Murtaza, S.-J. Dawson, D. W. Y. Tsui, D. Gale, T. Forshew, A. M. Piskorz, C. Parkinson, S.-F. Chin, Z. Kingsbury, A. S. C. Wong, F. Marass, S. Humphray, J. Hadfield, D. Bentley, T. M. Chin, J. D. Brenton, C. Caldas and N. Rosenfeld, *Nature*, 2013, **497**, 108-112.
33 Q. Zhou, J. Zheng, Z. Qing, M. Zheng, J. Yang, S. Yang, L. Ying and R. Yang, *Anal. Chem.*, **2016**, 88, 4759-4765.
34 J. Das, I. Ivanov, E. H. Sargent and S. O. Kelley, *J. Am. Chem. Soc.*, 2016, **138**, 11009-11016.
35 A. H. Nguyen and S. J. Sim, *Biosens. Bioelectron.*, 2015, **67**, 443-449.
36 P. Huang, F. Wu and L. Mao, *Anal. Chem.*, 2015, **87**, 6834-6841.
37 R. Nishiyabu, N. Hashimoto, T. Cho, K. Watanabe, T. Yasunaga, A. Endo, K. Kaneko, T. Niidome, M. Murata, C. Adachi, Y. Katayama, M. Hashizume and N. Kimizuka, *J. Am. Chem. Soc.*, 2009, **131**, 2151-2158.
38 C. Tang, Y. Bando, D. Golberg and R. Ma, *Angew. Chem. Int. Ed.*, 2005, **117**, 582-585.
39 X. Z. Wang, A. Lopez and J. W. Liu, *Langmuir*, 2018, **34**, 7899-7905.
40 C. X. Chen, Q. Yuan, P. J. Ni, Y. Y. Jiang, Z. L. Zhao and Y. Z. Lu, *Analyst*, 2018, **143**, 3821-3828.
41 H. H. Zeng, L. Zhang, L. Q. Rong, R. P. Liang and J. D. Qiu, *Biosens. Bioelectron.*, 2017, **89**, 721-727.

for TOC only

View Article Online
DOI: 10.1039/C9SC06408G

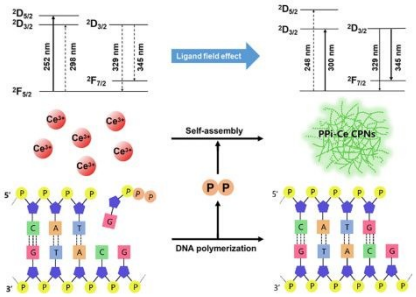

Textual abstract:

DNA polymerization is quantified by fluorescent pyrophosphate-cerium lanthanide coordination polymer networks, which is used to detect circulating tumor DNA sensitively.